Dual surface modifications of NiO_x/perovskite interface for enhancement of device stability

Jingyang Lin,[1,2] Yantao Wang,[1] Abdul Khaleed,[1] Ali Asgher Syed,[1] Yanling He,[1] Christopher C. S. Chan,[3] Yin Li,[1] Kuan Liu,[4] Gang Li,[4] Kam Sing Wong,[3] Jasminka Popović,[5] Jing Fan,[6] Alan Man Ching Ng,[2,*] and Aleksandra B. Djurišić[1,*]

[1] Department of Physics, The University of Hong Kong, Pokfulam Road, Hong Kong

[2]Dept. of Physics, Southern University of Science and Technology, No. 1088, Xueyuan Rd., Shenzhen, 518055, Guangdong, PR China.

[3]Dept. of Electronic and Information Engineering, The Hong Kong Polytechnic University, 11 Yuk Choi Rd, Hung Hom, Hong Kong

[4]Department of Physics, The Hong Kong University of Science and Technology, Clearwater Bay, Hong Kong.

[5]Ruđer Bošković Institute, Bijenička 54, 10000 Zagreb, Croatia

[6] Center for Computational Science and Engineering, Southern University of Science and Technology, No. 1088, Xueyuan Rd., Shenzhen, 518055, Guangdong, PR China.

ABSTRACT: Various phosphonic-acid based self-assembled monolayers (SAMs) have been commonly used for interface modifications in inverted perovskite solar cells. This typically results in significant enhancement of the hole extraction and consequent increase in the power conversion efficiency. However, the surface coverage and packing density of SAM molecules can vary, depending on the chosen SAM material and underlying oxide layer. In addition, different SAM molecules have diverse effects on the interfacial energy level alignment and perovskite film growth, resulting in complex relationships between surface modification, efficiency, and lifetime. Here we show that ethanolamine surface modification combined with [2-(9H-carbazol-9-yl)ethyl]phosphonic acid (2PACz) results in significant improvement in device stability compared to devices with 2PACz modification only. The significantly smaller size of ethanolamine enables it to fill any gaps in 2PACz coverage and provide improved interfacial defect passivation, while its different chemical structure enables it to provide complementary effects to 2PACz passivation. Consequently, the perovskite films are more stable under illumination (slower photoinduced segregation) and the devices exhibit significant stability enhancement. Despite similar power conversion efficiencies (PCE) between 2PACz only and combined ethanolamine-2PACz modification (PCE of champion devices ~21.6-22.0% for rigid and ~20.2-21.0% for flexible devices), the T80 lifetime under simulated solar illumination in ambient is improved more than 15 times for both rigid and flexible devices.

Keywords: halide perovskite; solar cells; interface modification; stability testing; flexible solar cells

INTRODUCTION

Inverted perovskite solar cells (PSCs) have been attracting increasing attention in recent years due to their simple fabrication, increased stability and lower hysteresis compared to conventional devices, which still retain efficiency advantage mainly due to improved charge extraction.[1-5] Among different materials used as hole transport layers (HTLs), NiO_x is commonly used,[2-15] since it results in improved stability compared to various organic HTL alternatives.[3,4,6,9] However, the efficiency of inverted PSCs with NiO_x HTL is limited by the low conductivity of NiO_x and the properties of NiO_x/perovskite interface.[3] Significant effort has consequently been made to improve the charge extraction in inverted PSCs, in particular those containing NiO_x HTL. Charge extraction improvement in NiO_x-containing inverted PSCs can be achieved by different approaches, such as doping as well as various surface functionalization with different molecules.[8] The use of surface modifications to improve hole extraction has an important advantage over doping, since it can also provide defect passivation at the NiO_x/perovskite interface.[5] One of the significant issues affecting the performance (efficiency and stability) of inverted PSCs with NiO_x is the presence of surface/interface defects, which can be detrimental to the device stability and cause perovskite degradation.[2,8,13] Various interfacial defects (Ni^{3+}, the presence of hydrates and other secondary phases) can also affect the growth of perovskite film and the formation of PbI_2 or NiI_2 upon light soaking.[8]

A variety of molecules has been used for surface modifications, including amines, thiols, carboxylates, and phosphonic acid containing molecules.[5-29] Among these, various phosphonic acid-based surface modifications are particularly promising due to the strong bonding of the phosphonate group to metal oxides, resulting in the widespread use of these types of molecules in PSCs,[6,10,14,16-27] as well as organic photovoltaics.[30-32] These molecules can bind to a variety of metal oxides, either by tridentate binding or a mixture of bidentate binding and hydrogen bonding.[30] Commonly used phosphonic acid-based surface modifiers include [2-(9H-carbazol-9-yl)ethyl]phosphonic acid (2PACz)[6,17,18,21-23,26,27] and MeO-2PACz ([2-(3,6-dimethoxy-9H-carbazol-9-yl)ethyl]phosphonic acid).[10,14,18,20,25,26] 2PACz in particular has been identified as a surface modifying molecule leading to favorable energy level alignment and significant suppression of interfacial defects in PSCs.[26]

However, the binding of the surface modifying molecules in general is known to be dependent on the imperfections of the surface, as well as the interactions among the molecules, which are affected by the rotations of the molecule backbones and changes in the tail group configurations.[20] It has been shown that MeO-2PACz exhibited inhomogeneous surface coverage on indium tin oxide (ITO).[10,19] It was also proposed that the large size of 2PACz molecules can lead to defects in packing and consequently surface coverage, so that metal oxide may be exposed between the neighboring molecules.[17] The coverage of surface modifying molecules is dependent on the hydroxyl group concentration on the surface, as the phosphonic acid group can bind to the surface hydroxyl group by condensation reaction.[10] The homogeneity and surface coverage were found to be improved by atomic layer deposition of NiO_x,[10] as well as sputtered NiO_x.[20] This has led to a significant reduction in the standard deviation of power conversion efficiency (PCE),[10] and/or improved efficiency.[20] Nevertheless, while NiO_x offers enhancement of strong tridentate binding compared to ITO,[20] it is still expected that there will be defects arising from unavoidable imperfect packing of molecules on any surface[24] and consequently exposed metal oxide surface.

One possible method to address this issue is to use co-adsorption of surface-modifying molecules. Co-adsorption of 2PACz with different molecules, such as methyl phosphonic acid[17] and MeOPACz[18,19] has been reported, with co-adsorption serving the purpose to improve surface coverage[17,19] or to tune energy level alignment utilizing different molecular dipoles of co-adsorbed molecules.[18] Other combinations of co-adsorbed layers include ((2,7-dimethoxy-9H-carbazol-9-yl) methyl) phosphonic acid and 6-(iodo-λ^5-azanyl) hexanoic acid.[24] The combination of other types of molecules, such as alkyl ammonium-based molecules, with phosphonic acid-based molecules can provide additional functionality, such as passivating defects in the perovskite in addition to covering any exposed metal oxide.[24] Thus, there is an interest in surface modifying molecules that can passivate defects in the perovskite by forming hydrogen bonds with inorganic lead halide octahedra,[5,24] and as a result various amino-group containing molecules have been reported for NiO_x surface modifications, such as 2-thiophenemethylamine[5] and diethanolamine.[7] It was also proposed that in the case of diethanolamine, N forms a bond with Ni, while the OH group interacts with uncoordinated Pb^{2+}.[7] Thus, ethanolamine-based

molecules have potential for interactions with both perovskite and NiO_x, which is beneficial for defect passivation.

Therefore, in this work we investigated NiO_x surface modification with 2PACz and ethanolamine (chemical structure of the two molecules is shown in **Figure S1**). The NiO_x nanoparticle layer could be deposited at low temperature and it is compatible with flexible substrates. While 2PACz provides excellent hole selectivity,[26] the ethanolamine molecule is expected to provide passivation of the perovskite and it is sufficiently small in size that it is expected to provide coverage of NiO_x surface not covered by 2PACz. Surprisingly, we have not found any significant enhancement of the efficiency or narrowing of the distributions of performance parameters with co-adsorption. However, dual surface modification was found to lead to substantial enhancement of the device stability, and device stability in general exhibited complex dependence on surface passivation as a consequence of interplay between interfacial defect passivation and energy level alignment across the device, as the buried interface modifications affect not only hole collection, but also electron collection.[6] It has been previously proposed that passivation of deep defects affects the efficiency, while the passivation of shallow defects affects the stability, and that immobilization of shallow point defects is not related to nonradiative recombination, so that devices with similar efficiencies can exhibit significantly different stability.[33] Different from using bulk additives,[33] here we show that different methods of NiO_x/perovskite interface passivation can have pronounced effect on device lifetime in devices with similar efficiencies. Our work contributes to improved understanding of the complex relationship between different types of defects, passivation molecules, interfacial energy level alignment, and solar cell performance (efficiency and stability).

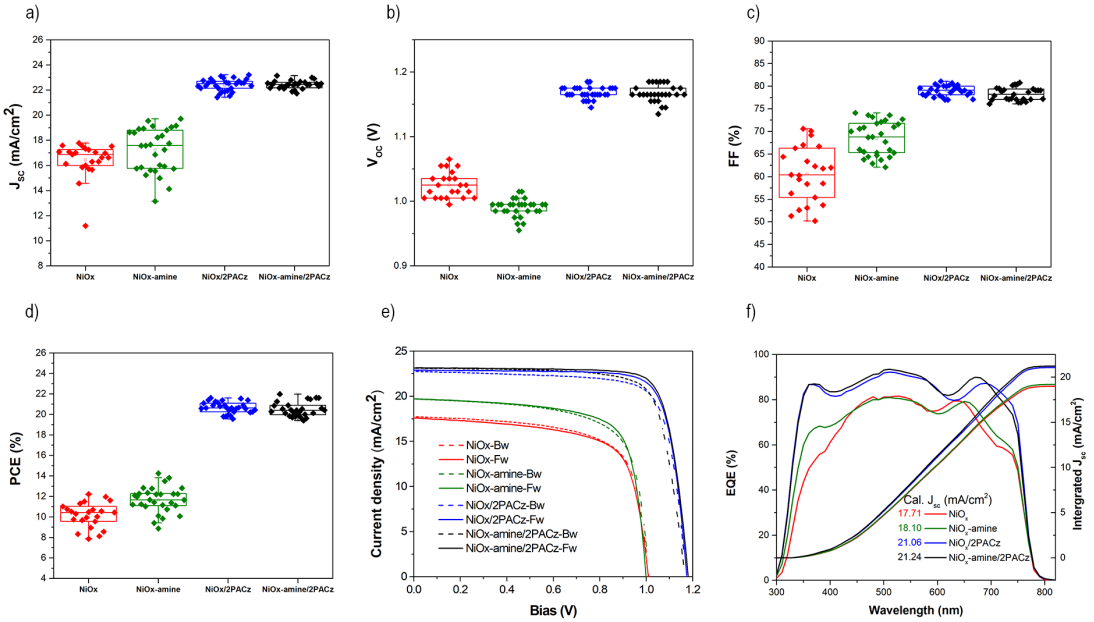

Figure 1. Performance parameters of PSCs with different NiO_x surface modifications (forward scan) a) J_{sc} b) V_{oc} c) FF and d) PCE; e) I-V curves under simulated solar illumination for forward scan (solid lines) and backward scan (dashed lines) f) EQE curves and corresponding integrated J_{sc} of PSCs with different NiO_x surface modifications.

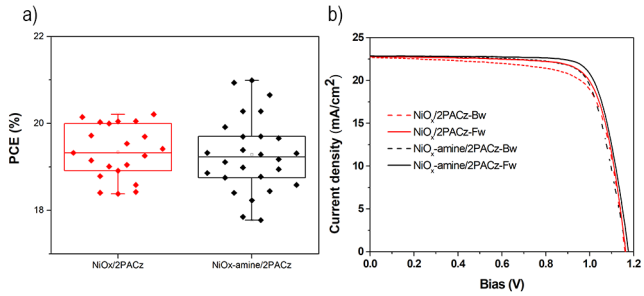

Figure 2 a) PCE distribution (forward scan) and b) I-V curves under forward (solid line) and backward (dashed line) scans of flexible PSCs with different NiO_x surface modifications.

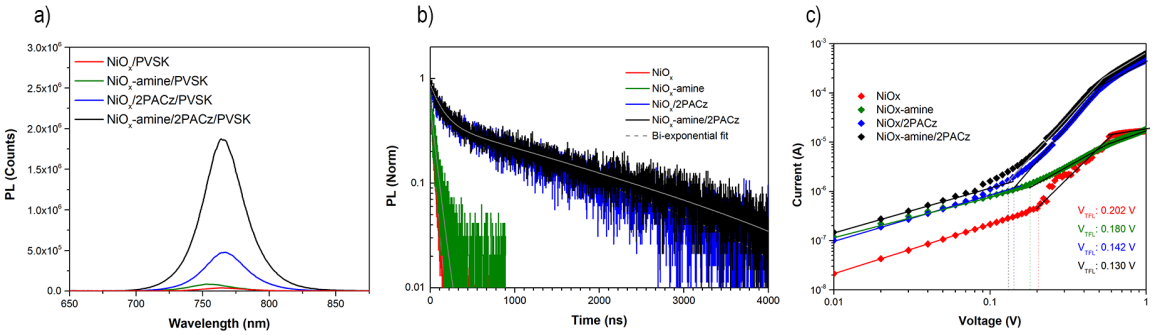

Figure 3 a) PL spectra and b) TRPL spectra of perovskite films on NiO_x with different surface modifications. c) SCLC curves of hole-only devices with different NiO_x surface treatments.

RESULTS AND DISCUSSION

To investigate the effect of NiO_x surface modifications, the concentrations of each molecule have been optimized, as shown in **Figure S2** and **S3**, and the effect of the sequence of modification was examined, as shown in **Figure S4**. In addition, since there are differences in performance trends of devices with 3D and 3D/2D perovskite layers on NiO_x with different surface modifications,[6] we prepared devices with PEAI top surface modification on top of 3D CsFAMA perovskite, with performance parameters, I-V curves and corresponding EQE curves shown in **Figure S1** and summarized in **Table S1**, and devices without PEAI top surface modifications, with performance parameters shown in **Figure S5**, and summarized in **Table S2**. Generally, similar trends are observed in devices with 3D/2D perovskite layer (**Figure 1, Table S1**) and devices with 3D perovskite layer (**Figure S5, Table S2**). However, it can be clearly observed that the NiO_x and NiO_x-amine devices with 3D perovskite exhibit higher PCE (mainly due to higher J_{sc}), while in the case of devices containing 2PACz modification 3D/2D PSCs have higher PCE. This is consistent with our previous work, where we found that 2PACz modification of NiO_x/perovskite interface leads to more favorable energy level alignment across 3D/2D/PCBM interface.[6] We can observe that the modification with ethanolamine (denoted as NiO_x-amine) results in an increase in J_{sc}, but a decrease in V_{oc}, leading to a PCE comparable to that of unmodified devices. An increase in J_{sc} is consistent with either improved charge extraction or reduced recombination losses, from which an increase in J_{sc} would also be expected. A possible cause of the reduced V_{oc} would be unfavorable surface dipole orientation, similar to the case previously observed for 2-thiophenemethylamine passivation, where surface dipoles and trap passivation resulted in opposite changes in V_{oc}.[5] Surface dipoles are expected at NiO_x/perovskite interface even without any modification, depending on the surface chemistry (defects, NiOOH species),[34,35] and the energy level alignment at that interface can be further changed by surface modifications, which in turn affects the V_{oc}. Different from NiO_x-amine, we can observe a significant increase in the V_{oc} in the devices containing 2PACz interface modification, in agreement with previous reports.[12,26] The samples with 2PACz interface modification also exhibit an increase in J_{sc}. The increase in short circuit current density can occur due to improved energy level alignment at the interfaces between the perovskite and charge transport layer,[6] as well as enhanced perovskite film quality.[7] It has been demonstrated that 2PACz modification results in a significant interface dipole and consequent changes in energy level alignment within the perovskite device,[6] which is likely responsible for the observed increase in J_{sc}. Similar performance is obtained for 2PACz only modification compared to amine-2PACz (slightly better champion device, similar average values) and similar performance trends to those on ITO/glass substrates are also observed for flexible devices, as shown in **Figure 2** and summarized in **Table S1**. It should be noted that for 3D perovskite active layer (**Figure S5**), small differences are observed in J_{sc} and FF trends for 2PACz only and amine-2PACz devices, but in this case as well the obtained efficiencies are similar. The hysteresis indices (HI), however, exhibit significantly different dependence on surface modifications in 3D (**Table S2**) and 3D/2D devices (**Table S1**). In both cases, for amine-2PACz we obtain a decrease in HI compared to unmodified NiO_x, but amine only and 2PACz only modifications exhibit higher HI compared to no modification for 3D/2D devices and lower HI compared to no modification for 3D devices. As hysteresis occurs due to charge accumulation at interfaces, caused by surface dipoles and/or unfavorable energy level alignment across the interface,[36-39] the reduction of hysteresis indicates a reduction in charge accumulation at interfaces during operation. Due to inherent differences in energy level alignment in devices with 3D and 3D/2D perovskite layers,[6] dependence of HI on surface modification of NiO_x differs for the case of 3D and 3D/2D perovskite. In the following, we will focus our investigation on the devices with 3D/2D layers, as this architecture leads to the best device performance for optimized interface modification.

To investigate the reasons for observed performance differences, we characterized the perovskite films and devices for different surface modifications of NiO_x. From XRD patterns, shown in **Supplementary Figure S6**, all samples contain 3D CsFAMA perovskite and some amount of hexagonal PbI_2. Diffraction lines belonging to ITO are also visible. The mixed cation 3D phase crystallizes in cubic P-43*m* space group with the unit-cell parameter $a = 6.269(7)$ Å which is in accordance with previous report.[40] The cell refinement was conducted by using structure published by Tian *et al.*[40] as a starting structural model while the A-site occupancies were modified constrained to $Cs_{0.05}FA_{0.79}MA_{0.16}$. For each sample, the area ratio of PbI_2(004) and 3D(001) diffraction lines was calculated and amount to: 0.4, 0.36, 0.28 and 0.22 for NiO_x, NiO_x-amine, NiO_x/2PACz and NiO_x-amine/2PACz, respectively. We can observe that the amount of PbI_2 phase is reduced in the case of surface modification which is in agreement with previous reports.[16] This is expected since increased PbI_2 presence is attributed to the instability of the perovskite/NiO_x interface,[8] since the surface defects induce redox reaction at the interface leading to the degradation of the perovskite.[2] Thus, the reduced presence of PbI_2 indicates increased interface stability and/or a reduction in interfacial defects. Therefore, we further investigated the charge collection and interfacial defect density in different samples. The photoluminescence (PL) and time-resolved photoluminescence (TRPL) spectra are shown in **Figure 3a** and **3b**, respectively, and the TRPL bi-exponential decay[4,6,11] fitting parameters are summarized in **Table S3**. Fast decay is typically attributed to the transfer of photogenerated holes to HTL, as well as surface recombination, whereas the slow decay component is commonly attributed to radiative bulk recombination in the perovskite film.[4,6] However, both fast and slow decay can be affected by trap passivation and charge transfer, resulting in complex relationships between trends observed in TRPL and device performance. For amine-NiO_x, we obtain a decrease in fast decay time and an increase in slow decay time, which indicates some defect passivation by ethanolamine and possibly a small improvement in hole extraction. While in the case of no 2PACz treatment, the changes in decay rates are within the same order of magnitude, for both cases containing 2PACz, dramatic increases in both decay times are observed. Increases in carrier lifetimes after surface modification with phosphonic acid-based molecules is in agreement with the previous reports,[6,18,26,27] as well as a significant increase in V_{oc} which is consistent with trap passivation and/or reduced recombination losses.[5] 2PACz was reported to passivate oxygen vacancies on NiO_x surface (with O atom of phosphoryl group filling the vacancy), while at the same time O from phosphoryl group can also form a bond with uncoordinated Pb^{2+}.[18] Thus, the significant increase in decay times is consistent with the proposed passivation effects of 2PACz. Higher PL intensity and longer decay times in the case of amine-2PACz compared to 2PACz indicates significant passivation of non-radiative defects, which would imply the reduction of non-radiative recombination. However, no significant differences in average solar cell performance are observed between these two modifications, although the champion devices exhibit higher efficiency for amine-2PACz. In addition to PL and TRPL, we have also performed additional characterization of charge transport. I-V curves of hole-only devices are shown in **Figure 3c**. After determining the trap filled limit voltage V_{TFL}, the trap density N_t can be determined as:[6,11]

$$N_t = \frac{2\varepsilon\varepsilon_0 V_{TFL}}{eL^2} \quad , \qquad (1)$$

where L is the thickness of the perovskite film, e is the elementary charge (1.602×10^{-19} C), ε is the relative dielectric constant, and ε_0 is the vacuum permittivity (8.8542×10^{-14} F/cm). The obtained values are summarized in **Table S4**, and the trap density trend $N_{untreated} > N_{amine} > N_{2PACz} > N_{amine\text{-}2PACz}$ is in agreement with the observed trends in PL and TRPL spectra.

In addition to these measurements, we have also attempted to further characterize charge transport by determining open circuit voltage dependence on illumination intensity to determine the ideality factor[6,21] and we performed C-V measurements to estimate defect densities from Mott-Schottky plots. Obtained results are shown in **Figure S7** and summarized in **Table S5**.

However, the results were different from the expectation and in contradiction with TRPL and SCLC results. Nevertheless, it is worth discussing the issue of the general applicability of common characterization techniques when investigating devices with interface modifications involving large interfacial dipoles and dramatic differences in contact selectivity. Let us discuss the ideality factor first. Ideality factor is governed by bulk as well as interfacial recombination properties.[21] In some but not all cases, high ideality factor values were reported for devices with phosphonic-acid based surface interface modification. For example, an ideality factor of 1.81 was previously reported for an inverted device employing 2PACz.[21] An increase in diode ideality factor upon surface modification with a phosphonic acid-based molecule was also observed in organic solar cells.[31] This was attributed to the fact that recombination can occur within the active layer (bulk recombination) or at the active layer/electrode interface (contact recombination).[31] In the case of bare metal oxide surface which contains hydroxyl groups that can act as traps, contact recombination dominates charge transport.[31] Surface modification was found to significantly suppress contact recombination, resulting in increased V_{oc} despite increased ideality factor.[31] From the observed significant increase in charge carrier lifetimes and an increase in V_{oc} in devices with 2PACz-modified NiO_x, interface recombination is likely significantly suppressed. Therefore, ideality factors of devices with and without 2PACz surface modification are not directly comparable, and caution is needed in the interpretation of the ideality factor derived from V_{oc} dependence on the illumination intensity. Devices exhibiting more than an order of magnitude difference in carrier lifetime, as

obtained in our work, likely cannot be directly compared to devices with more pronounced interfacial recombination. In general, the ideality factor value can be considered as an indication of trap-assisted recombination when the behavior is limited by recombination involving trapped charge carriers, rather than limited by surface/contact recombination.[41]

Similar to the ideality factor, the use of capacitance-voltage measurements and Mott-Schottky plots to determine defect densities in a device with a large interfacial dipole can also be problematic. From the Mott-Schottky plots shown in **Figure S2b**, we can observe increased built-in potential V_{bi} for devices with 2PACz and amine-2PACz interface modifications, consistent with additional electric field introduced by surface dipoles.[5] The increase in V_{bi} can also indicate a larger driving force for charge separation and reduced screening due to charges trapped at interfacial states.[6] However, the obtained defect densities are higher for 2PACz and amine-2PACz compared to untreated NiO_x and amine-NiO_x. It should be noted that standard models may not necessarily be applicable to structures containing ultrathin interfacial modifications, since the insulating molecules cannot be approximated by a pure capacitor due to the existence of a significant tunneling current.[42] In fact, tunneling has been specifically proposed as a mechanism of hole extraction with phosphonic acid-based interface modifications.[30,31] Therefore, a direct comparison of devices with and without 2PACz would not be appropriate for characterization techniques where there are significant differences in processes occurring in the devices.

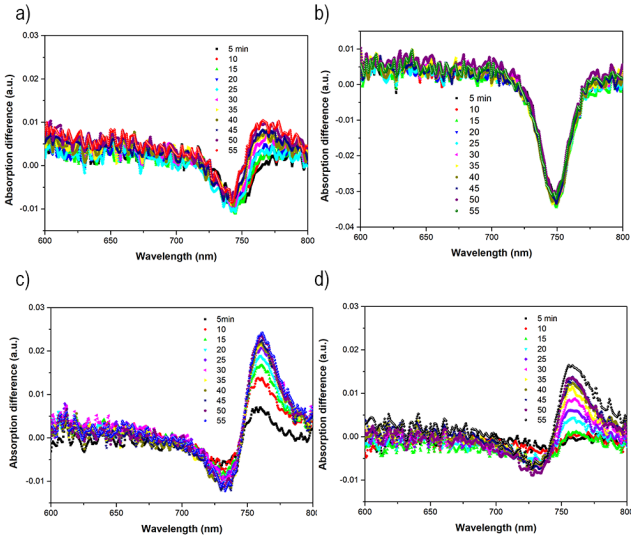

Figure 4. *In situ* absorption spectra difference under 1 Sun simulated solar illumination for perovskite films on a) NiO_x b) NiO_x-amine c) NiO_x/2PACz and d) NiO_x-amine/2PACz.

We can also observe from **Figure 3a** that there is a small shift in the position of the PL peak for different surface modifications of NiO_x, with peak position located at 766.1 nm in sample without modification, with blue shift observed for samples with amine modification (~756.0 nm for NiO_x-amine and ~765.6 for NiO_x-amine/2PACz) and a small red shift observed for NiO_x/2PACz (~766.8 nm). Different causes of blue or red shifts of PL peaks have been reported.[43-45] Blue shift of PL can occur due to passivation of trap levels near the band edge,[45] while red shift can occur due to photoinduced segregation of mixed halide perovskite.[44] Thus, observed blue shifts for ethanolamine passivated samples are consistent with trap passivation, consistent with TRPL and SCLC results. To examine the photoinduced segregation in the samples, we have performed *in-situ* absorption measurements to evaluate photoinduced segregation,[46] as shown in **Figure 4**. We see a lower level of photoinduced segregation in perovskite films on amine-2PACz modified NiO_x compared to NiO_x/2PACz, consistent with reduced defects and improved quality of the perovskite film. Interestingly, the photoinduced segregation in samples without surface modification is not very pronounced, while photoinduced segregation in NiO_x-amine samples exhibits quite unusual profile, i.e. we can observe a fast change in the absorption compared to initial value, but no further changes are evident as time increases. As hole trapping, followed by iodide oxidation and expulsion from the lattice, is responsible for photoinduced segregation,[47] we expect that photoinduced segregation would be affected by the concentration of hole traps, the efficiency of hole collection and consequently hole accumulation at interfaces. From the obtained values of fast decay constant in TRPL (**Table S3**), there are no indications of reduced efficiency of hole collection compared to bare NiO_x, consistent with increased J_{sc}. However, it should be noted that both fast decay constant and J_{sc} value are a result of interplay between multiple processes, and it is difficult to isolate any one contributing factor independently. One possible reason for unusual photoinduced segregation profile and significant magnitude of change in the absorption is the possibility of interaction between the amine group and the perovskite. It has been previously reported that molecules containing R-NH_2 can exhibit *in situ* protonation by FA when deposited on the perovskite.[48] This would however result in deprotonation of the organic cation in the perovskite, which is expected to result in increased ion migration.

Since the amine-containing surface modifications can also affect the quality of the perovskite film grown on top of the HTL,[7,35] we also examined the perovskite film quality and obtained cross-section SEM images are shown in **Figure S8**. We can observe that the use of ethanolamine results in increased fraction of grains extending from bottom-to-top of the perovskite films, compared to corresponding sample without ethanolamine. In contrast, 2PACz-modified films exhibit smaller grains along the cross-section. To understand in more detail the effects of passivation of two molecules, additional characterization of NiO_x with different passivation was conducted. It is known that defects on NiO_x surface can affect the stability of PSCs, as demonstrated by differences between oxygen-rich and oxygen-deficient NiO_x.[13] Thus, we have performed the XPS measurements of NiO_x modified with 2PACz only and amine-2PACz. From the Ni $2p_{3/2}$ spectra in **Figure S9,** we can observe that the ratio of the lowest energy peak at ~854 eV corresponding to Ni^{2+} (NiO) and the higher energy peak at ~856 eV corresponding to Ni^{3+} (NiOOH and Ni_2O_3)[5,13-15] is altered by surface modification, as summarized in **Table S6**. The broad higher energy peak is assigned to the satellite for NiO.[5,14,15] We can observe that the highest ratio is obtained for NiO_x-amine, indicating effective defect passivation in agreement with reduced trap density determined from SCLC measurements compared to NiO_x. We also observe an improvement in the Ni^{2+}/Ni^{3+} ratio for NiO_x-amine/2PACz compared to 2PACz only, also in agreement with the reduced trap density and increased TRPL decay time for NiO_x-amine/2PACz. The reduction in Ni^{3+} content is expected to result in improved stability.[13] O1s spectra can be fitted with three peaks, as shown in **Figure S10**, with the lowest energy peak (O1) corresponding to O^{2-} in the metal oxide lattice,[10,13] the O2 peak corresponds to surface hydroxyl groups including nickel hydroxide and nickel oxyhydroxide,[10,13,14] and lower coordination of oxygen in the presence of defects,[13,14] while the highest energy peak corresponds to adsorbed water and C=O.[10,13] In samples with 2PACz, P=O and Ni-P-O could also contribute to the O2 peak.[10] The analysis of the peak ratios in O 1s spectra is more complex since the higher energy peaks can arise both from surface defects and from functional groups present in the surface modifying molecule. For example, an increase in the peak at ~533 eV attributed to OH was observed after MeO-2PACz surface modifications, which could be attributed to the presence of OH groups in MeO-2PACz.[14] Thus, the presence of OH in the samples with ethanolamine surface modification can result in complex variations of peak ratios, since the defect passivation can lead to an increase in O1 relative to other peaks, while the presence of OH can result in a reduction on the relative strength of O1 peak. Nevertheless, from the changes in Ni^{2+}/Ni^{3+} ratios, we can unambiguously conclude that the surface modifications result in the reduction of defects on NiO_x surface, and that ethanolamine provides additional defect passivation, different from that obtainable by 2PACz modification. From FTIR spectra shown in **Figure S11**, we can also observe that ethanolamine is indeed present in both NiO_x-amine and NiO_x-amine/2PACz samples. While ethanolamine is less strongly bound to NiO_x compared to 2PACz based on DFT calculation (Supplementary Information, **Note S2** and **Figure S12**), from experimental results it is obvious that 2PACz modification does not displace all ethanolamine. The differences in the absorption of the two molecules are expected to contribute to the observed significant difference in device performance as a function of order of modification (**Figure S4**), as different fractions of ethanolamine and 2PACz on the surface are expected to be obtained for different order of modification.

It should also be noted that these two passivation molecules can have significantly different effects on the energy level alignment across the interface. The existence of surface dipoles at NiO_x surface is a complex issue, likely to depend on the method of preparation and any surface treatments (such as oxygen plasma). The presence of dipoles, enhanced by oxygen plasma, at NiO_x/ organic film interface was previously reported.[34] The magnitude of the dipoles can be significant, even exceeding 4 Debyes, while NH_2 group has opposing dipole moment, -4.5 Debyes.[35] The dipole moment of 2PACz was reported to be 2 Debyes.[26] Thus, we expect to observe significant differences in energy level alignment for these surface modifications. However, the energy level alignment across the interfaces in a device can be quite complex,[6,49,50] and the interface dipoles and vacuum level shifts are dependent not only on the dipole moments of modifying molecules, but also on their surface coverage, orientation, interfacial charge transfer, and trapping of charge carriers at self-assembled monolayer.[50] Thus, to examine the effects of energy band level alignment, UPS measurements were conducted. Energy level alignment is expected to affect not only efficiency, but also hysteresis index, photoinduced segregation,

and stability. We can observe vacuum level shifts for all device architectures considered, as shown in **Figure 5**. However, we can observe that there is a significant difference in the direction of the net vacuum level shift from perovskite to NiO_x for no modification and combined modification, as opposed to the single molecule modification.

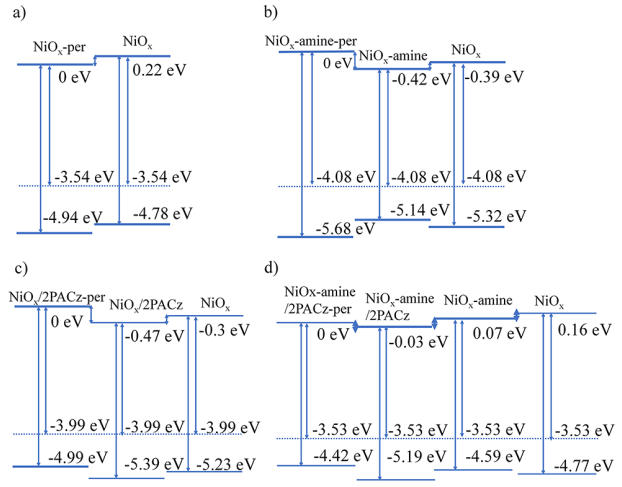

Figure 5. Illustration of energy level alignments obtained from UPS for different surface modifications of NiO_x assuming common Fermi level: a) bare NiO_x b) ethanolamine c) 2PACz and d) ethanolamine+2PACz.

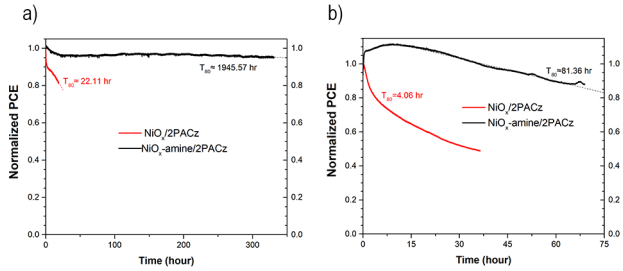

Figure 6. Normalized PCE under 1 Sun simulated solar illumination and MPP as a function of time for PSCs with different surface modifications a) rigid substrates b) flexible substrates.

Finally, we have performed stability testing at maximum power point (MPP) under 1 Sun simulated solar illumination. Obtained results for rigid and flexible substrates for NiO_x/2PACz and NiO_x-amine/2PACz are shown in **Figure 6a** and **6b**, respectively, while obtained results for rigid substrates for NiO_x and NiO_x-amine are shown in **Figure S13**. We can observe a very complex relationship between surface modification, device performance, and device stability. For NiO_x/2PACz and NiO_x-amine/2PACz devices, we can observe that even though devices exhibit similar efficiencies, different from previous reports on co-adsorbed monolayers,[24] significant difference in stability is obtained, with amine-2PACz exhibiting significant enhancement of stability. While short T_{80} (less than 24 h) is obtained in the case of 2PACz only (similar to a previous report of devices with 2PACz only HTL and 3D perovskite as an active layer which exhibited T_{80} of only 8h in nitrogen[21]), devices with amine-2PACz exhibited significant enhancement of the stability on both rigid and flexible substrates. It should be noted that the reports on the stability of flexible devices under illumination have been scarce, but it was reported that flexible tandem cells using 2PACz-MeO-PACz surface modifications retained 90% of initial efficiency after 150 h of illumination with an LED-based solar simulator.[18] While our flexible devices exhibit lower stability than that, the stability was measured under simulated solar illumination of a Xe-lamp based solar simulator which contains UV component, leading to reduced stability compared to a LED-based visible-light-only simulator.

Another interesting observation is shorter lifetime of the NiO_x-amine devices compared to unmodified NiO_x-amine. Possible reason for shorter lifetime is less efficient hole collection/hole accumulation, as this can lead to halide oxidation, ion migration/photoinduced segregation, and ultimately device degradation.[51,52] It has been reported that different HTLs[50] and different modifications[53] can result in significant differences in stability under illumination. From the energy level diagrams shown in **Figure 5**, we can observe a difference in the direction of vacuum level shift for samples exhibiting good stability (NiO_x and NiO_x-amine/2PACz) and samples exhibiting poor stability (NiO_x-amine, NiO_x/2PACz), indicating that existence of unfavorable interface dipoles and associated charge accumulation can result in detrimental effects on stability. There are also other possible contributing factors to the observed decrease in stability for amine-based surface modification, despite defect passivation on modified surface. Complex dependence between buried interface modifications, efficiency, and stability also occurs in part due to the coexistence of different deep and shallow defects, with deep defects affecting the efficiency, while shallow defects affect the ion migration and stability.[33,53,54] It was proposed that 2PACz passivation inhibits the formation of shallow traps at NiO_x/perovskite interface under UV illumination,[27] and that lower lifetime in devices with NiO_x without surface modifications could be attributed to NiO-induced deprotonation of organic cation.[27] NiO_x surface passivation could mitigate deprotonation, but different molecules resulted in different stability improvements.[27] Obviously, the stability trends would then depend on the initial properties of NiO_x. While ethanolamine passivates deep traps and improves the growth of the perovskite films, it has negative effects in the device stability when applied without other modifiers. Possible mechanism is that amine group induces deprotonation of the organic cation, which in turn destabilizes perovskite lattice under illumination and increases ion migration. It has been reported that PEAI surface modification results in increased interstitial iodine, and worsened the device stability, different from perovskite/HTL interface modification with a carbazole-pyridine based molecule.[53]

Thus, we can conclude that both ethanolamine and 2PACz interface modifications result in passivation of deep defects. Ethanolamine likely interacts more with the perovskite, and affects the growth of the film resulting in large vertical grains. The molecules also alter energy level alignment across the interface, which is favorable in case of 2PACz for the use of 3D/2D active layer. The less favorable energy level alignment for ethanolamine can lead to charge accumulation in the devices, resulting in worsening of the stability. Charge accumulation, combined with possible deprotonation of organic cation by the amine, is expected to lead to increased ion migration, in line with pronounced rapid photoinduced segregation and fast device performance degradation. Devices with 2PACz only also exhibit more pronounced phase segregation compared to devices without modification, likely due to inferior film morphology. The combination of ethanolamine and 2PACz enables their complementary action, with improved perovskite film quality compared to 2PACz only and lower defect density, while more favorable energy level alignment is obtained, resulting in not only high efficiency but also high stability.

CONCLUSIONS

We have investigated the effects of surface modifications of NiO_x with different molecules, namely ethanolamine and 2PACz, and their combination. We found that while ethanolamine can passivate defects at NiO_x surface, it worsens the device stability under illumination when used as sole interface modifier. In contrast, 2PACz provides excellent hole selectivity, leading to substantial increase in carrier lifetimes determined from TRPL measurements and improved photovoltaic performance. While comparable average efficiencies are obtained for 2PACz-only and amine-2PACz surface modifications, amine-2PACz interface modification results in a significant enhancement of stability under 1 Sun simulated solar illumination for both rigid and flexible devices, which can be attributed to improved perovskite layer quality and additional defect passivation provided by ethanolamine and adjustment in the energy level alignment for combined surface modification. In general, relationship between interface passivation, efficiency, and stability was found to be complex, arising from interplay between passivation of deep and shallow defects, perovskite growth on modified surface, energy level alignment across interfaces, and charge accumulation. Combination of molecules with complementary action addressing these issues can yield simultaneous optimization of both efficiency and stability.

ASSOCIATED CONTENT

Supporting Information. Tables summarizing photovoltaic performance, TRPL fitting, XPS fitting, defect densities estimated from different measurements, XRD patterns, XPS spectra, Mott-Schottky plots, V_{oc} dependence on illumination power. This material is available free of charge via the Internet at http://pubs.acs.org.

AUTHOR INFORMATION

Corresponding Authors

Alan Man Ching Ng: ngamc@sustech.edu.cn; Aleksandra B. Djurišić: dalek@hku.hk

Author Contributions

A. M. C. Ng and A. B. D. designed the whole study, analyzed and interpreted results and wrote the manuscript. J. Lin conducted the solar cell fabrication and characterization experiments, collected and summarized the experimental data, and Y. Li participated in device characterization. J. Popović analyzed XRD data. A. Khaleed synthesized NiO_x nanoparticles, A. A. Syed conducted the in-situ absorption experiment. Y. He conducted the XPS and UPS experiments as well as the peak fitting, and Y. T. Wang performed C-V measurements. C. C. S. Chan and K. S. Wong were responsible for PL and TRPL measurements, while K. Liu and G. Li provided EQE measurement. J. Fan performed DFT calculations. All co-authors provided input to the final version of the manuscript.

Notes

The authors declare no competing financial interest.

ACKNOWLEDGMENT

This work was supported by the PZS-2019-02-2068 project financed by the *"Research Cooperability"* Program of the Croatian Science Foundation and European Union from the European Social Fund under the Operational Programme Efficient Human Resources 2014-2020, the Seed Funding for Basic Research and Seed Funding for Strategic Interdisciplinary Research Scheme of the University of Hong Kong, RGC CRF project 7018-20G, and NSFC project 6207032617.

MATERIALS AND METHODS

Materials. All materials were used as received without further purification. Nickel (II) nitrate pentahydrate ($NiNO_3 \cdot 6H_2O$) was purchased from Duksan. Formamidinium iodide (FAI), methylammonium bromide (MABr), and phenethylammonium iodide (PEAI) were purchased from GreatCell Solar. Lead iodide (PbI_2), lead bromide ($PbBr_2$), [2-(9H-carbazol-9-yl)ethyl]phosphonic acid (2PACz), ethanolamine (2-Aminoethanol) were obtained from TCI. Sodium hydroxide (97%), Cesium iodide, N,N-Dimethylformamide (DMF), dimethyl sulfoxide (DMSO), and isopropanol (IPA) were purchased from Alfa Aesar. (6,6)-phenyl C61 butyric acid methyl ester (PCBM), bathocuproine (BCP) were purchased from Lumtec. Chlorobenzene (CB) was purchased from Aladdin. Methanol was purchased from Sigma-Aldrich. Chloroform (CF) was purchased from Acros.

NiO_x deposition and surface modification. NiO_x nanoparticles were prepared according to the previously published procedure.[15,16] Briefly, 6g of $NiNO_3 \cdot 6H_2O$ dissolved in 80 ml of de-ionized (DI) water and the clear solution was stirred vigorously. Then, 80 ml NaOH (1 mol/l in DI water) was dripped with the speed of 2-3 drops per second. The light green product of $Ni(OH)_2$ was collected via centrifugation on 10000 rpm after washing with DI water several times. Then, the $Ni(OH)_2$ powders were freeze-dried and annealed at 275 °C for 2 hr to obtain black NiO_x nanoparticles. The NiO_x nanoparticles powders were dispersed in DI water with the concentration of 20 mg/ml for HTL preparation.

Perovskite solar cells fabrication. The glass-ITO and PEN-ITO (Peccell 15 Ω sq-1) substrates (25×25 mm^2) were cleaned by detergent (Decon 90, 1% in DI water), DI water and ethanol by sonication for 15 min in each solvent sequentially. The washed substrates were blow dried with N_2 and treated with oxygen plasma at 10 V for 15 s. HTL was prepared via spin coating NiO_x nanoparticle ink at 3000 rpm for 40 s onto the cleaned substrate, followed by annealing at 110 °C for 10 min. Amine modification was realized by spin coating ethanolamine solution (1:50 v: v in ethanol) onto as prepared NiOx/ITO substrate at 4000 rpm for 30 s and annealing at 100 °C for 5 min. Samples with coated NiO_x (with or without amine modification) were then transferred to a glove box. For 2PACz modification, 2PACz solution (0.5 mg/ml in IPA) was spin coated at 4000 rpm for 30 s and annealed at 100 °C for 10 min. Active layer was CsFAMA perovskite, as reported previously.[55] Briefly, 18.2 mg CsI, 172 mg FAI, 22.4 mg MABr, 507.1 mg PbI_2 and 73.4 mg $PbBr_2$ dissolved in 1 ml DMF: DMSO (4:1 v: v) solvent and stirred at 60ºC for 90 mins before use. Perovskite layer deposition was performed by one-step spin-coating at 4000 rpm for 35s. At 10 s after the start, 300 µl of CB antisolvent was dropped onto the perovskite film. The perovskite film was annealed at 110 °C for 40 min. To obtain a 2D top layer, PEAI solution (1 mg/ml in IPA) was spin coated on top of CsFAMA perovskite at 5000 rpm for 30s, followed by annealing at 100 °C for 3 min. Electron transport later was deposited by spin coating PCBM solution (20 mg/ml in CB) at 1200 rpm for 30 s followed by annealing at 100 °C for 10 min. BCP interlayer was deposited by spin coating at 4000 rpm for 30s without annealing. Finally, 100 nm Ag was evaporated through a shadow mask to obtain a device with the electrode area of 0.09 cm^2 (3 mm x 3 mm). As-prepared perovskite solar cells were encapsulated with polyisobutylene (PIB) and a cover glass.

Characterization. XRD patterns were measured using a Rigaku MiniFlex600 with Cu Kα X-ray source in θ-2θ scan mode with step of 0.01° from 10° to 55°. Capacitance-voltage curves were measured by a CHI660C electrochemical workstation. EQE was measured with a Enli QE-R 3011 EQE system. UV-vis absorption spectra were measured with a Cary 60 UV-vis spectrophotometer. Steady-state PL measurements were obtained with a CVI Melles Griot LC500 HeCd (325 nm) laser as excitation and PL spectra collected with a PDA-512USB fiberoptic spectrometer. The XPS and UPS measurement were performed using an ESCA-LAB 250xi (Thermo Fisher). The C1s binding energy (284.8 eV) was used as energy reference during the XPS measurements. The photoelectrons in UPS measurements were excited using a He lamp with an energy of 21.22 eV and a resolution of 0.05 eV. Excitation source for TRPL measurement was a 635 nm 100-picosecond laser diode (Edinburgh Instruments) with switchable repetition rates operating at 1 MHz and 200KHz. The excitation intensity (at the glass substrate side) was ≈15 nJ cm^{-2}. The PL was collected by a monochromator (Acton SpectraPro 275), and the center wavelength was sent into a photon counter at the exit port, where time correlated single photon counting was performed using a Becker and Hickl system (SPC150). SEM was measured by Hitachi S-4800. ATR-FTIR was measured by PerkinElmer Spectrum Two. Details of calculations are given in SI, Note S2.

I-V measurements were performed using a Keithley 2400 source measure unit under 1 sun illumination with 100 mW/cm^2 intensity and AM1.5G spectrum (ABET Sun 2000 solar simulator with calibration by Enli PVM silicon standard reference cell). All solar cell devices were measured after encapsulation in ambient condition (room temperature, RH 60-70 %) using an aperture mask of 0.04 (0.2× 0.2) cm^2. I-V scan was performed with step of 0.01 V and 10 ms delay. Backward scan was performed from 1.2 V to -0.2V and forward scan was performed from -0.2 V to 1.2 V. Maximum power point (MPP) testing for stability evaluation under illumination was measured under the same environment as mentioned above.

REFERENCES

1. Cacovich, S.; Vidon, G.; Degani, M.; Legrand, M.; Gouda, L.; Puel, J. B.; Vaynzof, Y.; Guillemoles, J. F.; Ory, D.; Grancini, G. Imaging and Quantifying Non-Radiative Losses at 23% Efficient Inverted Perovskite Solar Cells Interfaces. *Nat. Commun.* **2022**, *13*, 2868.

2. Cui, X.; Jin, J.; Zou, J.; Tang, Q.; Ai, Y.; Zhang, X.; Wang, Z.; Zhou, Y.; Zhu, Z.; Tang, G.; Cao, Q.; Liu, S.; Liu, X.; Tai, Q. NiO_x Nanocrystals with Tunable Size and Energy Levels for Efficient and UV Stable Perovskite Solar Cells. *Adv. Funct. Mater.* **2022**, *32*, 2203049.

3. Shen, G.; Cai, Q.; Dong, H.; Wen, X.; Xu, X.; Mu, C. Using Interfacial Contact Engineering to Solve Nickel Oxide/Perovskite Interface Contact Issues in Inverted Perovskite Solar Cells. *ACS Sustainable Chem. Eng.* **2021**, *9*, 3580-3589.

4. Wang, Z.; Rong, X.; Wang, L.; Wang, W.; Lin, H.; Li, X. Dual Role of Amino-Functionalized Graphene Quantum Dots in NiO_x Films for Efficient Inverted Flexible Perovskite Solar Cells. *ACS Appl. Mater. Interfaces* **2020**, *12*, 8342-8350.

5. Hu, Y.; Yang, Z.; Cui, X.; Zeng, P.; Li, F.; Liu, X.; Feng, G.; Liu, M. Construction of Charge Transport Channels at the NiO_x/Perovskite Interface through Moderate Dipoles toward Highly Efficient Inverted Solar Cells. *ACS Appl. Mater. Interfaces* **2022**, *14*, 13431-13439.

6. Wang, Y.; Lin, J.; He, Y.; Zhang, Y.; Liang, Q.; Liu, F.; Zhou, Z.; Chan, C. C. S.; Li, G.; Feng, S.-P.; Ng, A. M. C.; Wong, K. S.; Popović, J.; Djurišić, A. B. Improvement in the Performance of Inverted 3D/2D Perovskite Solar Cells by Ambient Exposure. *Sol. RRL* **2022**, *6*, 2200224.

7. Bai, Y.; Chen, H.; Xiao, S.; Xue, Q.; Zhang, T.; Zhu, Z.; Li, Q.; Hu, C.; Yang, Y.; Hu, Z.; Huang, F.; Wong, K. S.; Yip, H.-L.; Yang, S. Effects of a Molecular Monolayer Modification of NiO Nanocrystal Layer Surfaces on Perovskite Crystallization and Interface Contact toward Faster Hole Extraction and Higher Photovoltaic Performance. *Adv. Funct. Mater.* **2016**, *26*, 2950-2958.

8. Di Girolamo, D.; Di Giacomo, F.; Matteocci, F.; Marrani, A. G.; Dini, D.; Abate, A. Progress, Highlights and Perspectives on NiO in Perovskite Photovoltaics. *Chem. Sci.* **2020**, *11*, 7746-7759.

9. Roose, B.; Wang, Q.; Abate, A. The Role of Charge Selective Contacts in Perovskite Solar Cell Stability. *Adv. Energy Mater.* **2019**, *9*, 1803140.

10. Phung, N.; Verheijen, M.; Todinova, A.; Datta, K.; Verhage, M.; Al-Ashouri, A.; Kobler, H.; Li, X.; Abate, A.; Albrecht, S.; Creatore, M. Enhanced Self-Assembled Monolayer Surface Coverage by ALD NiO in p-i-n Perovskite Solar Cells. *ACS Appl. Mater. Interfaces* **2022**, *14*, 2166-2176.

11. Fu, Y.; Liu, X.; Zhao, S. Mandelic Acid as an Interfacial Modifier for High Performance NiO_x-based Inverted Perovskite Solar Cells. *ChemNanoMat* **2022**, *8*, e202200091.
12. Das, C.; Kedia, M.; Zuo, W.; Mortan, C.; Kot, M.; Ingo Flege, J.; Saliba, M. Band Bending at Hole Transporting Layer-Perovskite Interfaces in n-i-p and in p-i-n Architecture. *Sol. RRL* **2022**, *6*, 2200348.
13. Haider, M. I.; Fakharuddin, A.; Ahmed, S.; Sultan, M.; Schmidt-Mende, L. Modulating Defect Density of NiO Hole Transport Layer via Tuning Interfacial Oxygen Stoichiometry in Perovskite Solar Cells. *Solar Energy* **2022**, *233*, 326-336.
14. Alghamdi, A. R. M.; Yanagida, M.; Shirai, Y.; Andersson, G. G.; Miyano, K. Surface Passivation of Sputtered NiO_x Using a SAM Interface Layer to Enhance the Performance of Perovskite Solar Cells. *ACS Omega* **2022**, *7*, 12147-12157.
15. Chen, W.; Wu, Y.; Fan, J.; Djurišić, A. B.; Liu, F.; Tam, H. W.; Ng, A.; Surya, C.; Chan, W. K.; Wang, D.; He, Z.-B. Understanding the Doping Effect on NiO: Toward High-Performance Inverted Perovskite Solar Cells. *Adv. Energy Mater.* **2018**, *8*, 1703519.
16. Chen, W.; Zhu, Y.; Xiu, J.; Chen, G.; Liang, H.; Liu, S.; Xue, H.; Birgersson, E.; Ho, J. W.; Qin, X.; Lin, J.; Ma, R.; Liu, T.; He, Y.; Ng, A. M.-C.; Guo, X.; He, Z.; Yan, H.; Djurišić, A. B.; Hou, Y. Monolithic Perovskite/Organic Tandem Solar Cells with 23.6% Efficiency Enabled by Reduced Voltage Losses and Optimized Interconnecting Layer. *Nature Energy* **2022**, *7*, 229-237.
17. Kapil, G.; Bessho, T.; Sanehira, Y.; Sahamir, S. R.; Chen, M.; Baranwal, A. K.; Liu, D.; Sono, Y.; Hirotani, D.; Nomura, D.; Nishimura, K.; Kamarudin, M. A.; Shen, Q.; Segawa, H.; Hayase, S. Tin–Lead Perovskite Solar Cells Fabricated on Hole Selective Monolayers. *ACS Energy Lett.* **2022**, *7*, 966-974.
18. Li, L.; Wang, Y.; Wang, X.; Lin, R.; Luo, X.; Liu, Z.; Zhou, K.; Xiong, S.; Bao, Q.; Chen, G.; Tian, Y.; Deng, Y.; Xiao, K.; Wu, J.; Saidaminov, M. I.; Lin, H.; Ma, C.-Q.; Zhao, Z.; Wu, Y.; Zhang, L.; Tan, H. Flexible all-perovskite tandem solar cells approaching 25% efficiency with molecule-bridged hole-selective contact. *Nature Energy* **2022**, *7,* 708-717.
19. Mishima, R.; Hino, M.; Kanematsu, M.; Kishimoto, K.; Ishibashi, H.; Konishi, K.; Okamoto, S.; Irie, T.; Fujimoto, T.; Yoshida, W.; Uzu, H.; Adachi, D.; Yamamoto, K. 28.3% Efficient Perovskite-Silicon Tandem Solar Cells with Mixed Self-Assembled Monolayers. *Appl. Phys. Exp.* **2022**, *15*, 076503.
20. Sun, J.; Shou, C.; Sun, J.; Wang, X.; Yang, Z.; Chen, Y.; Wu, J.; Yang, W.; Long, H.; Ying, Z.; Yang, X.; Sheng, J.; Yan, B.; Ye, J. NiO_x-Seeded Self-Assembled Monolayers as Highly Hole-Selective Passivating Contacts for Efficient Inverted Perovskite Solar Cells. *Sol. RRL* **2021**, *5*, 2100663.
21. Gharibzadeh, S.; Fassl, P.; Hossain, I.; Rohrbeck, P. N.; Frericks, M.; Schmidt, M.; Duong, T.; Khan, M. R.; Abzieher, T.; Abdollahi Nejand, B.; Schackmar, F.; Almora, O.; Feeney, T.; Singh, R.; Fuchs, D.; Lemmer, U.; Hofmann, J. P.; Weber, S.; Paetzold, U. W. Two Birds with One Stone: Dual Grain-Boundary and Interface Passivation Enables > 22% Efficient Inverted Methylammonium-Free Perovskite Solar Cells. *Energy Environ. Sci*. **2021**, *14*, 5875-5893.
22. Dagar, J.; Fenske, M.; Al-Ashouri, A.; Schultz, C.; Li, B.; Kobler, H.; Munir, R.; Parmasivam, G.; Li, J.; Levine, I.; Merdasa, A.; Kegelmann, L.; Nasstrom, H.; Marquez, J. A.; Unold, T.; Tobbens, D. M.; Schlatmann, R.; Stegemann, B.; Abate, A.; Albrecht, S.; Unger, E. Compositional and Interfacial Engineering Yield High-Performance and Stable p-i-n Perovskite Solar Cells and Mini-Modules. *ACS Appl. Mater. Interfaces* **2021**, *13*, 13022-13033.
23. Huang, Y.; Liu, T.; Li, D.; Lian, Q.; Wang, Y.; Wang, G.; Mi, G.; Zhou, Y.; Amini, A.; Xu, B.; Tang, Z.; Cheng, C.; Xing, G. Bridging the Interfacial Contact for Improved Stability and Efficiency of Inverted Perovskite Solar Cells. *Small* **2022**, *18*, 2201694.
24. Deng, X.; Qi, F.; Li, F.; Wu, S.; Lin, F. R.; Zhang, Z.; Guan, Z.; Yang, Z.; Lee, C. S.; Jen, A. K. Co-assembled Monolayers as Hole-Selective Contact for High-Performance Inverted Perovskite Solar Cells with Optimized Recombination Loss and Long-Term Stability. *Angew. Chem. Int. Ed.* **2022**, *61*, e202203088.
25. Wong, M. H.; An, Q.; Kress, J.; Mörsdorf, J.-M.; Ballmann, J.; Vaynzof, Y. Surface Dipole Assisted Charge Carrier Extraction in Inverted Architecture Perovskite Solar Cells. *Appl. Phys. Lett.* **2021**, *119*, 233903.
26. Al-Ashouri, A.; Magomedov, A.; Roß, M.; Jošt, M.; Talaikis, M.; Chistiakova, G.; Bertram, T.; Márquez, J. A.; Köhnen, E.; Kasparavičius, E.; Levcenco, S.; Gil-Escrig, L.; Hages, C. J.; Schlatmann, R.; Rech, B.; Malinauskas, T.; Unold, T.; Kaufmann, C. A.; Korte, L.; Niaura, G.; Getautis, V.; Albrecht, S. Conformal Monolayer Contacts with Lossless Interfaces for Perovskite Single Junction and Monolithic Tandem Solar Cells. *Energy Environ. Sci*. **2019**, *12,* 3356-3369.
27. Zhu, X. L.; Lau, C. F. J.; Mo, K. W.; Cheng, S. Y.; Xu, Y. L.; Li, R. M.; Wang, C.; Zheng, Q. X.; Liu, Y.; Wang, T.; Lin, Q. Q.; Wang, Z. P. Inverted Planar Heterojunction Perovskite Solar Cells with High Ultraviolet Stability. *Nano Energy* **2022**, *103*, 107849.
28. Liu, Y. N.; Duan, J. J.; Zhang, J. K.; Huang, S. M.; Ou-Yang, W.; Bao, Q. Y.; Sun, Z.; Chen, X. H. High Efficiency and Stability of Inverted Perovskite Solar Cells Using Phenethyl Ammonium Iodide-Modified Interface of NiO_x and Perovskite Layers. *ACS Appl. Mater. Interfaces* **2020**, *12*, 771−779.
29. Zhang, J. K.; Luo, H.; Xie, W. J.; Lin, X. H.; Hou, X.; Zhou, J. P.; Huang, S. M.; Ou-Yang, W.; Sun, Z.; Chen, X. H. Efficient and Ultraviolet Durable Planar Perovskite Solar Cells via a ferrocenecarboxylic acid modified Nickel Oxide Hole Transport Layer. *Nanoscale* **2018**, *10*, 5617.
30. Paniagua, S. A.; Giordano, A. J.; Smith, O. L.; Barlow, S.; Li, H.; Armstrong, N. R.; Pemberton, J. E.; Bredas, J. L.; Ginger, D.; Marder, S. R. Phosphonic Acids for Interfacial Engineering of Transparent Conductive Oxides. *Chem. Rev.* **2016**, *116*, 7117-7158.
31. Wang, H.; Gomez, E. D.; Guan, Z.; Jaye, C.; Toney, M. F.; Fischer, D. A.; Kahn, A.; Loo, Y.-L. Tuning Contact Recombination and Open-Circuit Voltage in Polymer Solar Cells via Self-Assembled Monolayer Adsorption at the Organic–Metal Oxide Interface. *J. Phys. Chem. C* **2013**, *117*, 20474-20484.
32. MacLeod, B. A.; Horwitz, N. E.; Ratcliff, E. L.; Jenkins, J. L.; Armstrong, N. R.; Giordano, A. J.; Hotchkiss, P. J.; Marder, S. R.; Campbell, C. T.; Ginger, D. S. Built-In Potential in Conjugated Polymer Diodes with Changing Anode Work Function: Interfacial States and Deviation from the Schottky-Mott Limit. *J. Phys. Chem. Lett.* **2012**, *3,* 1202-1207.
33. Xie, H. B.; Wang, Z. W.; Chen, Z. H.; Pereyra, C.; Pols, M.; Gałkowski, K.; Anaya, M.; Fu, S.; Jia, X. Y.; Tang, P. Y.; Kubicki, D. J.; Agarwalla, A.; Kim, H.-S.; Prochowicz, D.; Borrisé, X.; Bonn, M.; Bao, C. X.; Xiaoxiao Sun, X. X.; Zakeeruddin, S. M.; Emsley, L.; Arbiol, J.; Gao, F.; Fan Fu,F.; Wang, H. I.; Tielrooij, K.-J.; Stranks, S. D.; Tao, S. X.; Grätzel, M.; Hagfeldt, A.; Lira-Cantu, M. Decoupling the Effects of Defects on Efficiency and Stability Through Phosphonates in Stable Halide Perovskite Solar Cells, Joule **2021**, *5*, 1246–1266.
34. Ratcliff, E. L.; Meyer, J.; Steirer, K. X.; Armstrong, N. R.; Olson, D.; Kahn, A. Energy Level Alignment in PCDTBT:$PC_{70}BM$ Solar Cells: Solution Processed NiO_x for Improved Hole Collection and Efficiency. *Org. Electron.* **2012**, *13*, 744-749.
35. Cheng, Y. H.; Li, M. L.; Liu, X. X.; Cheung, S. H.; Chandran, H. T.; Li, H. W.; Xu, X. W.; Xie, Y. M.; Soe, S. K.; Yip, H. L.; Tsang, S. W. Impact of Surface Dipole in NiO_x on the Crystallization and Photovoltaic Performance of Organometal Halide Perovskite Solar Cells. *Nano Energy* **2019**, *61*, 496-504.
36. Galatopoulos, F.; Papadas, I. T.; Ioakeimidis, A.; Eleftheriou P.; Choulis, S. A. Surface Treatment of Cu:NiO_x Hole-Transporting Layer Using β-Alanine for Hysteresis-Free and Thermally Stable Inverted Perovskite Solar Cells. *Nanomaterials* **2020**, *10*, 1961.
37. Guerrero, A.; Bou, A.; Matt, G.; Almora, O.; Heumüller, T.; Garcia-Belmonte, G.; Bisquert, J.; Hou, Y.; Brabec, C. Switching Off Hysteresis in Perovskite Solar Cells by Fine-Tuning Energy Levels of Extraction Layers. *Adv. Opt. Mater.* **2018**, *8*, 1703376.
38. García-Rodríguez, R.; Riquelme, A. J.; Cowley, M.; Valadez-Villalobos, K.; Oskam, G.; Bennett, L. J.; Wolf, M. J.; Contreras-Bernal, L.; Cameron, P. J.; Walker, A. B.; Anta, J. A. Inverted Hysteresis in n–i–p and p–i–n Perovskite Solar Cells. *Energy Technol.* **2022**, *10*, 2200507.
39. Liu, J.; Yin, X. T.; Guo, Y. X.; Que, M. D.; Chen, J.; Chen, Z.; Que, W. X.; Influence of Hole Transport Layers/Perovskite Interfaces on the Hysteresis Behavior of Inverted Perovskite Solar Cells. *ACS Appl. Energy Mater.* **2020**, *3*, 6391−6399.
40. Chen, L.; Tan, Y. Y.; Chen, Z. X.; Wang, T.; Hu, S.; Nan, Z. A.; Xie, L. Q.; Hui, Y.; Huang, J. X.; Zhan, C.; Wang, S. H.; Zhou, J. Z.; Yan, J. W.; Mao, B. W.; Tian, Z. Q. Toward Long-Term Stability: Single-Crystal Alloys of Cesium-Containing Mixed Cation and Mixed Halide Perovskite, J. Am. Chem. Soc. 2019, 141, 4, 1665–1671.
41. Ju, D.; Zhao, T.; Dang, Y.; Zhang, G.; Hu, X.; Cui, D.; Tao, X. Gas Induced Conversion of Hybrid Perovskite Single Crystal to Single Crystal for

Great Enhancement of Their Photoelectric Properties. *J. Mater. Chem. A* **2017**, *5*, 21919-21925.
42. Vilan, A.; Cahen, D. Chemical Modification of Semiconductor Surfaces for Molecular Electronics. *Chem. Rev.* **2017**, *117*, 4624-4666.
43. Kim, H. S.; Hagfeldt, A. Photoinduced Lattice Symmetry Enhancement in Mixed Hybrid Perovskites and Its Beneficial Effect on the Recombination Behavior. *Adv. Optical Mater*. **2019**, *7*, 1801512.
44. Gautam, S.K.; Kim, M. J.; Miquita, D. R.; Bourée, J. E.; Geffroy, B.; Plantevin, O. Reversible Photoinduced Phase Segregation and Origin of Long Carrier Lifetime in Mixed-Halide Perovskite Films. *Adv. Funct. Mater.* **20**, *30*, 2002622.
45. Hwang, T.; Yun, A. J.; Lee, B.; Kim, J.; Lee, Y.; Park, B. Methylammonium-Chloride Post-Treatment On Perovskite Surface and Its Correlation to Photovoltaic Performance in the Aspect Of Electronic Traps. J. Appl. Phys. **2019**, *126*, 023101.
46. Nandi, P.; Li, Z.; Kim, Y.; Ahn, T. K.; Park, N.-G.; Shin, H. Stabilizing Mixed Halide Lead Perovskites against Photoinduced Phase Segregation by A-Site Cation Alloying. *ACS Energy Lett.* **2021**, *6,* 837-847.
47. DuBose, J. T.; Kamat, P. V.Hole Trapping in Halide Perovskites Induces Phase Segregation. *Acc. Mater. Res*. **2022**, *3*, 761−771.
48. Zhu, Z. J.; Mao, K. T.; Zhang, K.; Peng, W.; Zhang, J. Q.; Meng, H. G.; Cheng, S.; Li, T. Q.; Lin, H. Z.; Chen, Q.; Wu, X. J.; Xu, J. X. Correlating the Perovskite/Polymer Multi- Mode Reactions with Deep-Level Traps in Perovskite Solar Cells. *Joule* **2022**, *6*, 2849–2868.
49. Duhm, S. Interface Energetics Make Devices. *Electron. Struct.* **2022**, *4* 034003.
50. Zojer, E.; Taucher, T. C.; Hofmann, O. T. The Impact of Dipolar Layers on the Electronic Properties of Organic/Inorganic Hybrid Interfaces. *Adv. Mater. Interfaces* **2019**, *6,* 1900581.
51. Bertoluzzi, L.; Patel, J. B.; Bush, K. A.; Boyd, C. C.; Kerner, R. A.; O'Regan, B. C.; McGehee, M. D. Incorporating Electrochemical Halide Oxidation into Drift-Diffusion Models to Explain Performance Losses in Perovskite Solar Cells under Prolonged Reverse Bias. *Adv. Energy Mater.* **2021**, *11*, 2002614.
52. Sekimoto, S.; Matsui, T.; Nishihara, T.; Uchida, R.; Sekiguchi, T.; Negami, T. Influence of a Hole-Transport Layer on Light-Induced Degradation of Mixed Organic−Inorganic Halide Perovskite Solar Cells. *ACS Appl. Energy Mater.* **2019**, *2*, 5039−5049.
53. Tumen-Ulzii, G.; Auffray, M.; Klotz, D.; Harrington, G. F.; Chen, X. K.; Balijapalli, U.; Vediyappan, V.; Nakamura, N.; Feng, Z.; Takekuma, K.; Fujita, Y.; Wang, P. P.; Yamada, S.; Tamada, K.; Batmunkh, M.; Zhong, Y. L.; Mathevet, F.; Salway, H.; Anaya, M.; Stranks, S. D.; Matsushima, T.; Adachi, C. Defect Passivation by Pyridine-Carbazole Molecules for Efficient and Stable Perovskite Solar Cells. ACS Appl. Energy Mater.. 2022, 5, 15819-15827
54. Chen, B.; Rudd, P. N.; Yang, S.; Yuan, Y. B.; Huang, J. S. Imperfections and Their Passivation in Halide Perovskite Solar Cells. *Chem. Soc. Rev.* **2019**, *48*, 3842-3867.
55. Saliba, M.; Matsui, T.; Seo, J. Y.; Domanski, K.; Correa-Baena, J. P.; Nazeeruddin, M. K.; Zakeeruddin, S. M.; Tress, W.; Abate, A.; Hagfeldt, A.; Gratzel, M. Cesium-Containing Triple Cation Perovskite Solar Cells: Improved Stability, Reproducibility and High Efficiency. *Energy Environ. Sci.* **2016**, 9, 1989-1997.